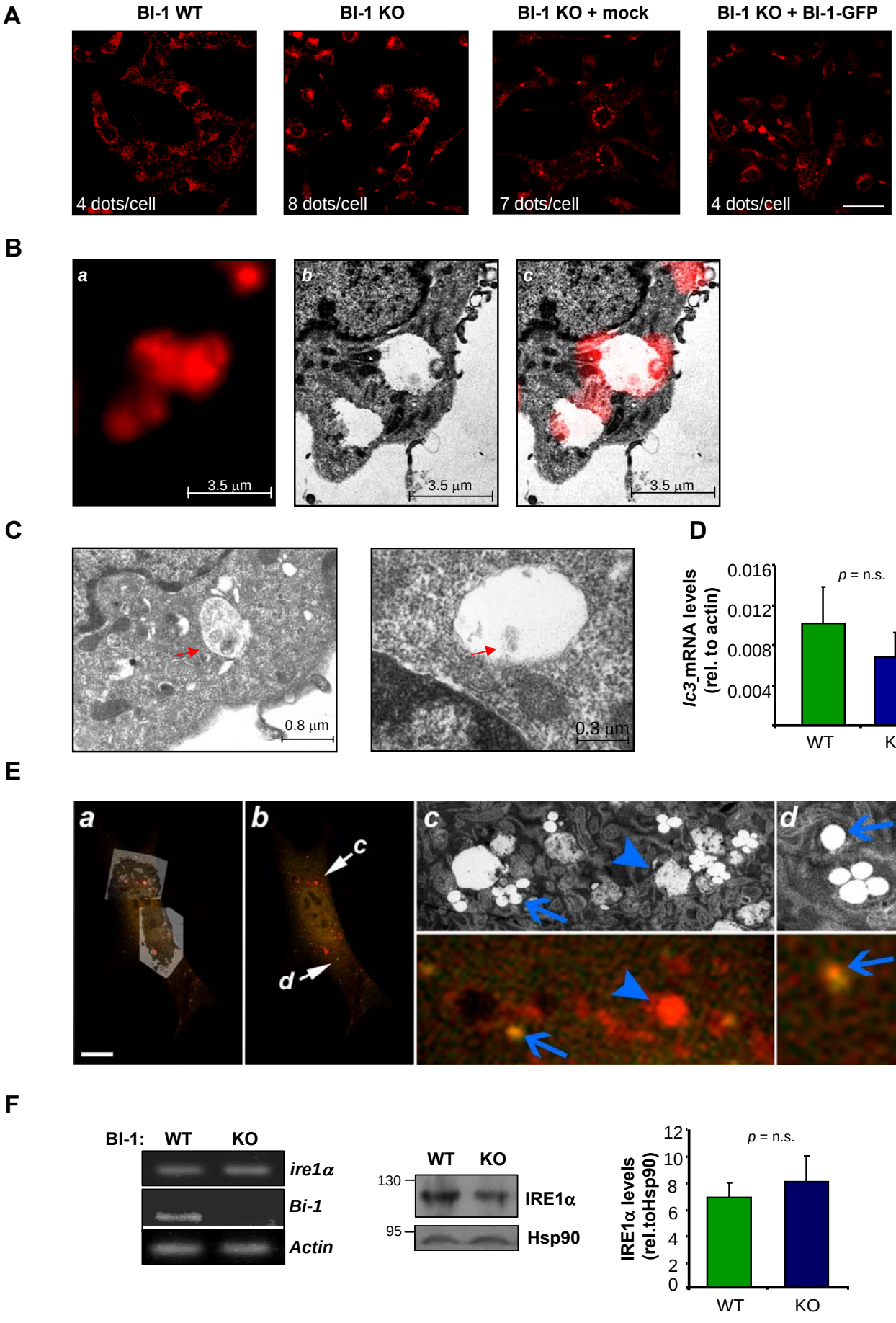

Castillo et al., Fig. S1

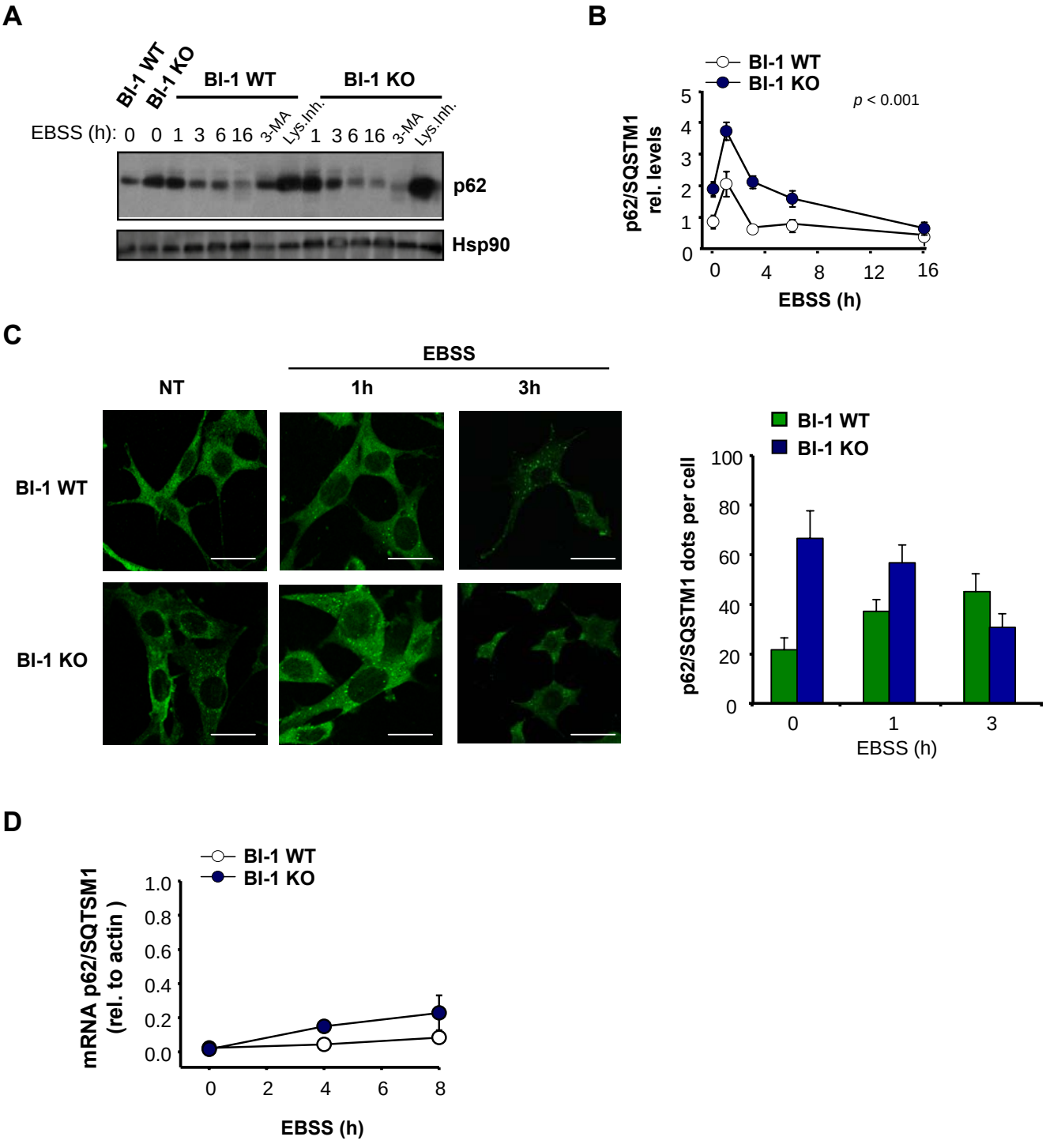
A
Bl-1 WT
Bl-1 KO
Bl-1 WT
Bl-1 KO
EBSS (h): 0 0 1 3 6 16 3-MA Lys.Inh. 1 3 6 16 3-MA Lys.Inh.
p62
Hsp90
B
Bl-1 WT
Bl-1 KO
p < 0.001
p62/SQSTM1 rel. levels
EBSS (h)
C
EBSS
NT
1h
3h
Bl-1 WT
Bl-1 KO
Bl-1 WT
Bl-1 KO
p62/SQSTM1 dots per cell
EBSS (h)
D
Bl-1 WT
Bl-1 KO
mRNA p62/SQTSM1 (rel. to actin)
EBSS (h)

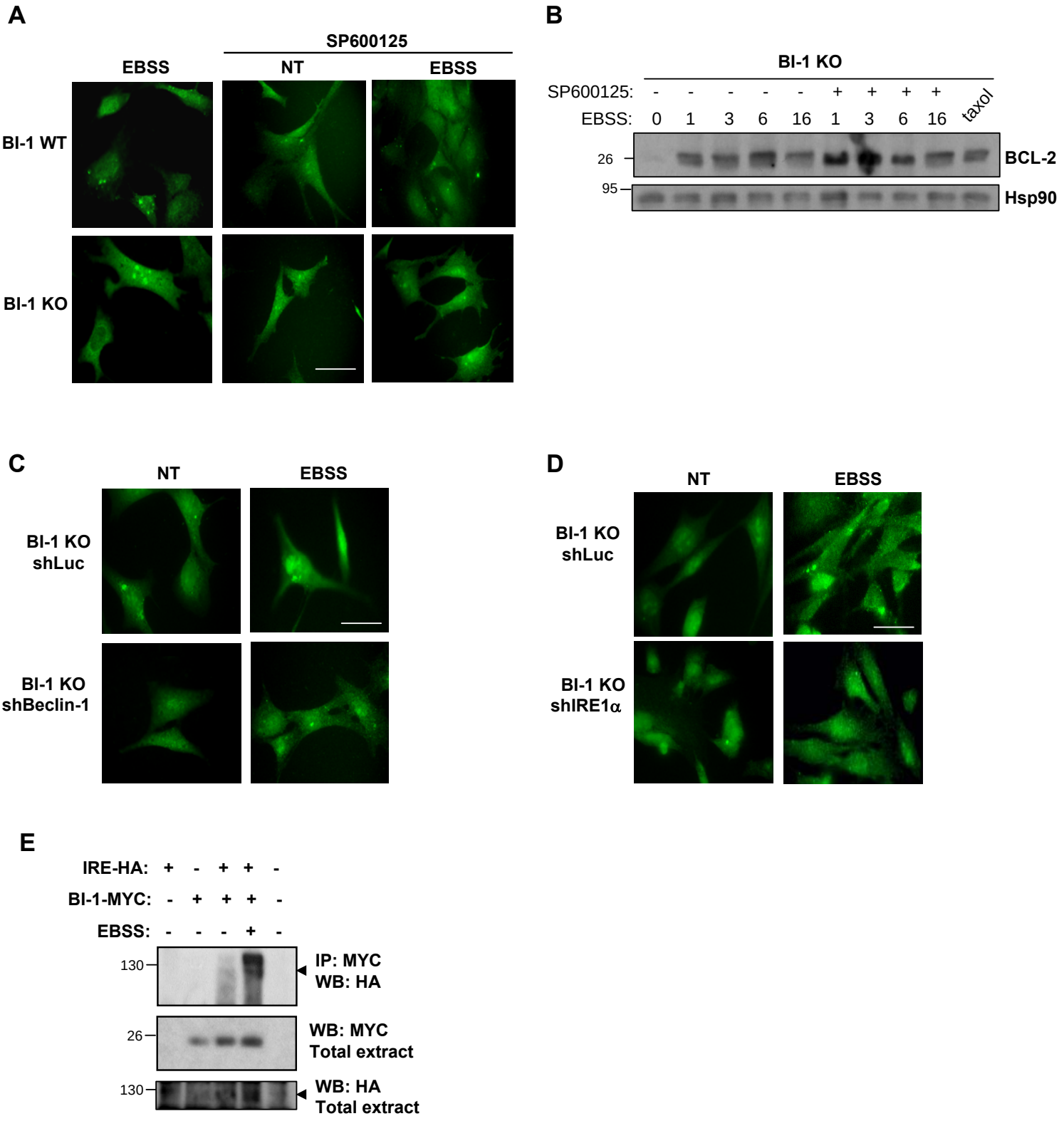
A
SP600125
EBSS
NT
EBSS
Bl-1 WT
Bl-1 KO
B
Bl-1 KO
SP600125: - - - - - + + + +
EBSS: 0 1 3 6 16 1 3 6 16 taxol
26
95
BCL-2
Hsp90
C
NT
EBSS
Bl-1 KO shLuc
Bl-1 KO shBeclin-1
D
NT
EBSS
Bl-1 KO shLuc
Bl-1 KO shIRE1α
E
IRE-HA: + - + + -
Bl-1-MYC: - + + + -
EBSS: - - - + -
130
IP: MYC
WB: HA
26
WB: MYC
Total extract
130
WB: HA
Total extract

A

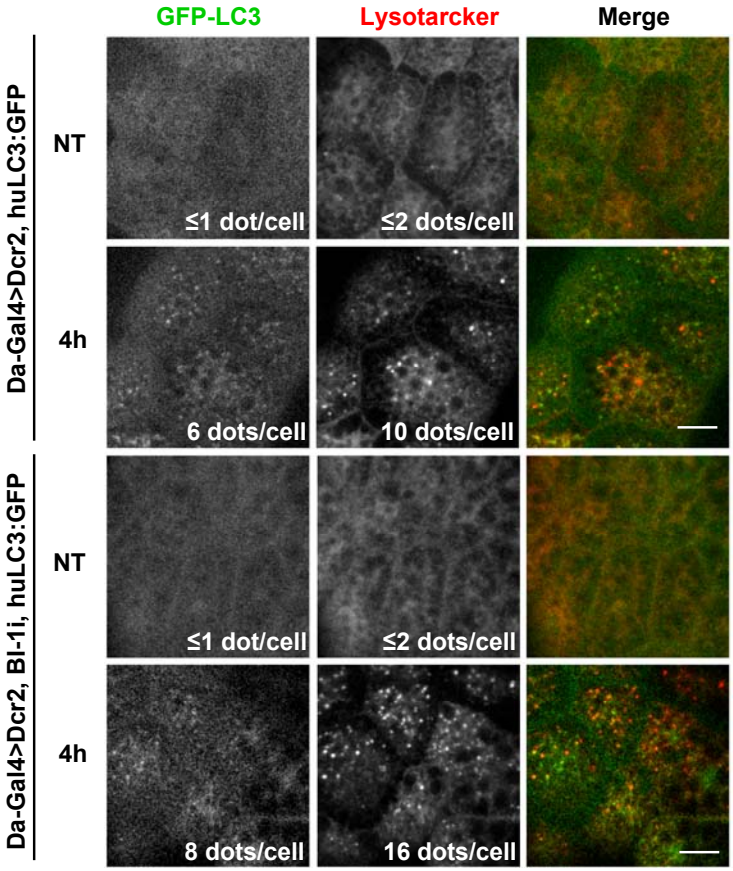
GFP-LC3
Lysotarcker
Merge
Da-Gal4>Dcr2, huLC3:GFP
NT
≤1 dot/cell
≤2 dots/cell
4h
6 dots/cell
10 dots/cell
Da-Gal4>Dcr2, BI-1i, huLC3:GFP
NT
≤1 dot/cell
≤2 dots/cell
4h
8 dots/cell
16 dots/cell

B

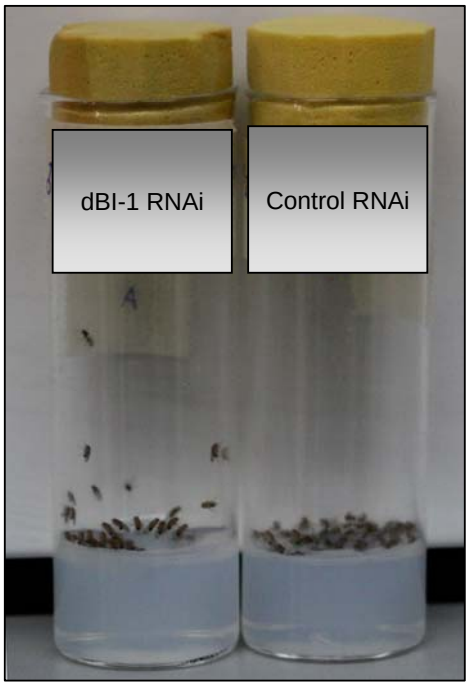
dBI-1 RNAi
Control RNAi

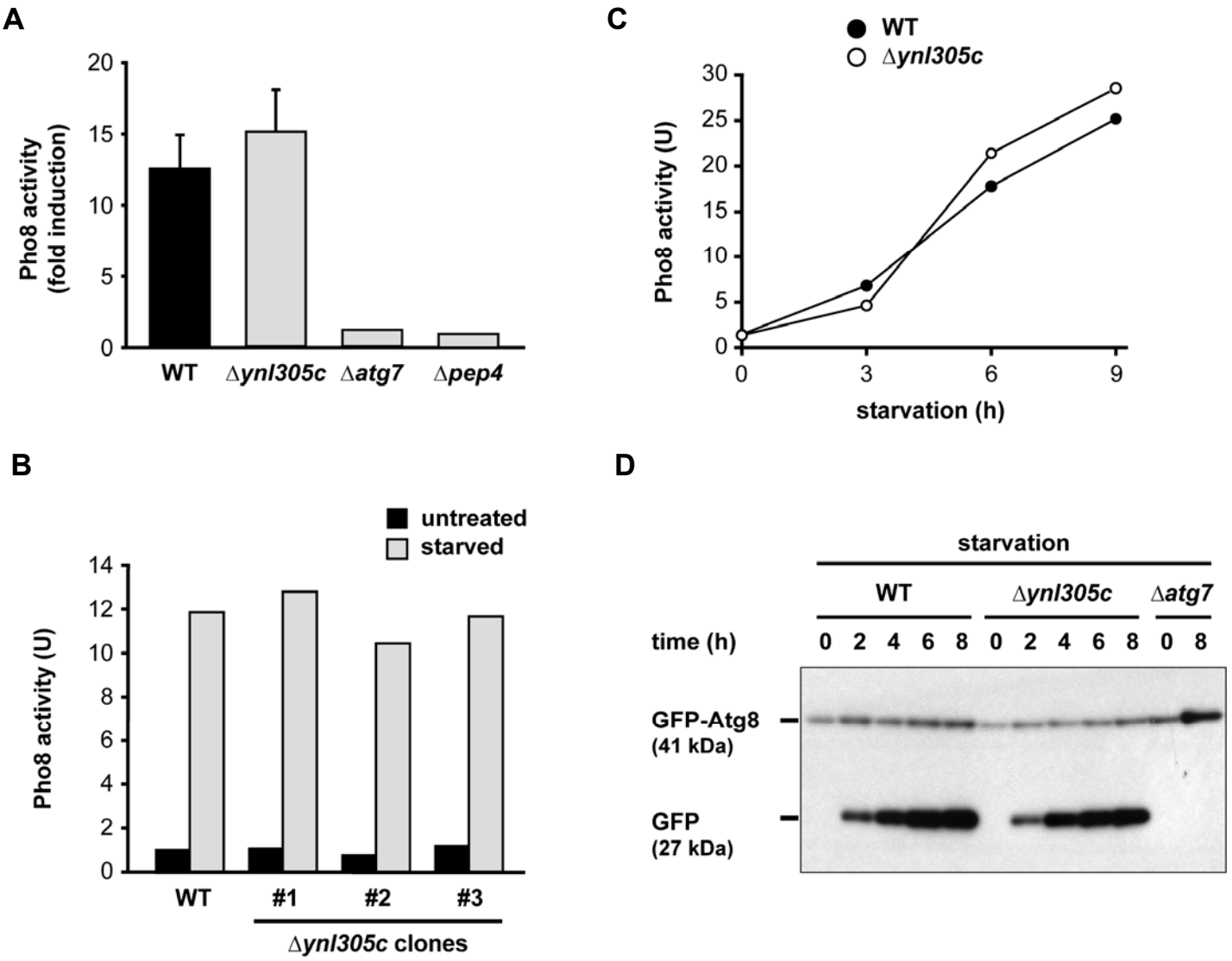

Castillo et al., Fig. S5

Supplementary material

Figure S1. Visualization of acidic vesicles by correlative fluorescent and electron microscopy of BI-1 KO MEFs exposed to starvation. (**A**) BI-1 WT and KO MEFs cells were stained with lysotracker (red), and observed with a confocal microscope. In addition, BI-1 KO cells were stably transduced with retroviruses expressing BI-1-GFP or empty vector (mock). Then the number of large lysotracker-positive dots per cell were quantified (insets, N= 40 cells per conditions). Scale bar: 20 μm. (**B**) High magnification of lysotracker positive vacuoles (right panel), EM images of the same cell (middle panel), and co-localization of both images (right panel). (**C**) *Left*: High magnification electron micrographs of large vesicles observed in BI-1 deficient cells under starvation in an intermediate stage of autophagy, characterized by the presence of abundant electron dense material in the vesicle lumen. *Right*: Late stage autophagic vesicle of BI-1 KO cells subjected to starvation showing small amount of cargo material. (**D**) *lc3* mRNA levels were monitored in BI-1 WT and KO cells by real time PCR. Data represents mean and standard deviation of three independent experiments. n.s.: non significant differences. **(E)** BI-1 KO cells were transiently transfected with an expression vector for a monomeric-tandem LC3-RFP-GFP construct. After 24h, cells were exposed to EBSS for 3 h. Then, autophagy fluxes were monitored in living cells by visualizing the distribution of LC3 positive dots in the red and green channel using a confocal microscopy. Then, EM analysis was performed of the same cells to visualize the presence of vesicular structures with co-localization with fluorescent imaged. In ***a*,** co-localization between fluorescent (merged green and red channels) and EM images is presented. Scale bar: 10 μm. ***b***, Arrows indicate LC3-RFP-GFP dots that are then analyzed with higher magnification. ***c***, ***d***, Two examples for the analysis of EM (upper panels) and fluorescent images (lower panel) with higher magnifications. Arrows and arrowheads indicate the visualization of red and yellow dots. **(F)** IRE1α mRNA levels were monitored by semi-quantitative PCR in BI-1 WT and KO

MEFs. Right panel: In addition IRE1α expression was determined by Western blot analysis. Data represents mean and standard deviation of three independent experiments. n.s. non significant differences.

Figure S2. Degradation of p62/SQSTM1 in BI-1 deficient cells undergoing autophagy. (**A**) BI-1 WT and KO MEFs were treated with EBSS for indicated time points and the levels of p62/SQSTM1 were determined by Western blot analysis. Hsp90 levels were monitored as loading control. In addition, cells were treated with a cocktail of lysosomal inhibitors (200 nM bafilomycin A_1, 10 μg/ml pepstatin and E64d; lys. inh) to monitor the basal degradation of p62/SQSTM1 in BI-1 WT and KO cells. In addition, treatment with 10 mM 3-MA was used as control. (**B**) Quantification of p62/SQSTM1 levels relative to Hsp90 was performed in experiments presented in A. Mean and standard deviation are presented representative of three independent experiments. Two-way ANOVA test was used to analyze statistical significance. (**C**) Endogenous p62/SQSTM1 distribution was assessed in BI-1 WT and KO cells by immunofluorescence under basal conditions or after stimulation with EBSS for indicated time points. Right panel: Quantification of the number of p92-positive dots per cell. Analysis represents the visualization of at lest 90 cells. Scale bar: *Upper*: left 20 μm, middle 10 μm, right 20 μm; *Lower*: left 10 μm, middle 10 μm, right 30 μm. (**D**) Determination of *p62* mRNA levels in cells treated as with EBSS for indicated time points determined using real time PCR. Mean and standard deviation are presented of three determinations representative of two independent experiments.

Figure S3. The induction of autophagy by BI-1 depends on JNK, Beclin-1 and IRE1α. In (**A**), (**C**) and (**D**), representative images are shown corresponding to quantifications presented in Figures 4B, 5C and 5D respectively. Scale bars: 20 μm. (**B**) BI-1 KO cells

were treated with EBSS in presence or absence of SP600125 for indicated tome points, and the electrophoretic shift related to BCL-2 phosphorylation was determined by Western blot. As positive control of BCL-2 phosphorylation shift, cells were treated with 5 μM taxol, which induced JNK-mediated phosphorylation. (**E**) 293T cells were co-transfected with expression vectors for HA-tagged IRE1α (IRE1-HA), and MYC-tagged BI-1 (BI1-MYC). After 48 h of transfection, cells were exposed or not to EBSS for 4 h and HA-tagged proteins were immunoprecipitated and analyzed by Western blot.

Figure S4. BI-1 controls autophagy activation in *Drosophila melanogaster*. (**A**) LC3-GFP distribution was monitored in control (DaGal4>huLC3:GFP) or dBI-1 knockdown larvae (DaGal4>huLC3:GFP, Dcr2, dBI-1i) under basal conditions or after exposure to nutrient starvation for 4 h. Pictures were acquire from non-fixed fat tissues. In addition, lysotracker staining was performed to visualize lysosomes. Quantification of the average number of LC3-GFP or lysotracker positive dots per cell is indicated as insets (N = 10). Scale bars: 20 μm. (**B**) Control or dBI-1 RNAi adult flies were exposed to nutrient starvation and then animal viability was visualized after 120 h of nutrient starved. Note: Dead flies are observed in the bottom of the tube whereas living flies tend to move into the top of the tube.

Figure S5. Ynl305c does not regulate starvation-induced autophagy in yeast. (**A**) Pho8Δ60-expressing wild-type (WT; n = 3), Δ*ynl305c* (n = 3), Δ*atg7* (n = 1), and Δ*pep4* (n = 1) yeast were left untreated or starved of nitrogen for 9 h. Pho8Δ60 activity was measured as described in Materials and Methods and expressed as fold induction after starvation. Average and standard error are shown where applicable. (**B**) Pho8Δ60-expressing wild-type (WT) yeast and three Δ*ynl305c* clones were left untreated or starved of nitrogen for 9 h. Pho8Δ60 activity was measured and expressed in enzymatic units (U).

(**C**) Pho8Δ60-expressing WT and Δ*ynl305c* yeast (clone #1) were left untreated or starved of nitrogen for the indicated times, and Pho8Δ60 activity was measured and expressed as above. **(D)** WT, Δ*ynl305c* and Δ*atg7* cells expressing GFP-Atg8 under the *ATG8* promoter were starved of nitrogen for the indicated times and analyzed by Western blotting using an anti-GFP antibody. Upon starvation, the GFP-Atg8 fusion protein is delivered to yeast lysosomes by autophagy. Lysosomal proteases then quickly degrade Atg8 while the more compactly folded GFP persists. The accumulation of free GFP therefore serves as an indicator of autophagy. As can be seen, free GFP accumulates to a similar extent in wild-type and Δ*ynl305c* cells but not in autophagy-defective Δ*atg7* cells. Note that starvation activates the *ATG8* promoter and results in an overall increase of GFP signal.